Thermal conduction in a harmonic chain coupled to two cavity-optomechanical systems

Ziqiang He and Guangjiong Dong

State Key Laboratory of Precision Spectroscopy, School of Physics and Material Science, East China Normal University, Shanghai 200062, China

and Collaborative Innovation Center of Extreme Optics, Shanxi University, Taiyuan, Shanxi 030006, China

(Received 28 January 2021; accepted 2 April 2021; published 12 May 2021)

We propose a model including a one-dimensional harmonic chain of oscillators whose two ends coupled two cavity-optomechanical systems for studying one-dimensional thermal conductivity in statistical physics. In this model, the cavity-optomechanical systems function as two laser-engineerable thermal reservoirs. When the effective temperatures of the two reservoirs are not equal, a heat flux through the chain can be generated, and moreover the classical and quantum features of the heat flux have been studied. We further show that the heat flux does not obey the Fourier's law in this model. The thermal switching phenomenon could be induced by controlling the on-site vibrational frequency. Finally, we propose to apply the correlation between two mechanical oscillators to measure the heat flux through the chain.

DOI: 10.1103/PhysRevA.103.053509

I. INTRODUCTION

Cavity optomechanics has made remarkable progress in studying the crossover from classical physics to quantum physics [1–3], and precision measurement [4–15] . Over the last few years, the study of thermal physics with cavity-optomechanical systems, such as the quantum heat engine [16–19] and persistent thermal flux [20,21], has emerged as a new frontier of this subject.

In thermal physics, one important topic is to understand the Fourier's law for the heat transport in temperature gradient systems from first principles [22,23]. Theoretical analysis shows that the Fourier's law could be violated in lower-dimensional systems, demonstrated as size-dependent thermal conductivity (a ratio of the heat flux over the temperature gradient) [24–36]. Experimental demonstration of the anomaly of Fourier's law [37] is important for nonequilibrium stochastic physics and thermal engineering in low-dimensional systems.

With the theoretical progress in the investigation of the Fourier's law, a wealth of possibilities for the transport, control, and rectification of heat in the physical reality of the nanosystems have been explored. For example, thermal diodes [38–40], thermal switching effect [41,42], and thermal logic gates [43], as well as thermal memories [44], have been proposed. The experimental realization [45,46] of these devices can greatly enrich nanophononics [47].

The experimental progress of laser cooling and trapping particles could facilitate the testing of the lattice models used in low-dimensional heat transport theory [48–54]. In this way, laser-cooled particles at the two ends of the chain are analogous to reservoirs. However, the cooling lasers need to tightly focused to a regime less than one lattice period. Moreover, how to measure the thermal flux is a challenge. For a chain of trapped ions, Ref. [53] proposes a spin wave to monitor the heat flux, yet to be experimentally demonstrated. Recently, heat transport between optomechanically coupled nanomechanical resonators and between hydrodynamically coupled particles trapped in water by optical tweezers has also been proposed and experimentally realized [21,55].

In this paper, we note that a cavity-optomechanical system can function as a thermal reservoir that can be engineered by a driving laser [16,18–20]; we thus propose to apply two cavity-optomechanical systems at unequal effective temperatures, respectively, to couple to two ends of a chain of harmonic oscillators for investigating heat transport problems in low-dimensional systems. The heat flux approaches a constant value as the particle number increases, showing breakdown of the Fourier's law in this system, in agreement with previous research on thermal conductivity in harmonic chains [22–25,28]. The heat flux can be controlled by the driving lasers and on-site potential, which provide high flexibility for experimentally testing lattice models and investigating low-dimensional heat conduction problems in this system. Moreover, the heat flux can be measured by the correlation of the two mechanical oscillators in the cavity-optomechanical systems.

The paper is organized as follows. In Sec. II, we present our model and obtain quantum fluctuations of the oscillators and the electromagnetic field. We further calculate the heat flux through the chain and study its properties in Sec. III. In Sec. IV, we propose a scheme using the cross correlation of the mechanical oscillators to measure heat flux. In Sec. V, we present a summary.

II. THEORETICAL MODEL FOR THE HYBRID SYSTEM OF A HARMONIC CHAIN COUPLED TO TWO CAVITY-OPTOMECHANICAL SYSTEMS AT TWO ENDS

Our model, shown in Fig. 1, is a chain composed of N trapped identical particles of mass m whose two ends,

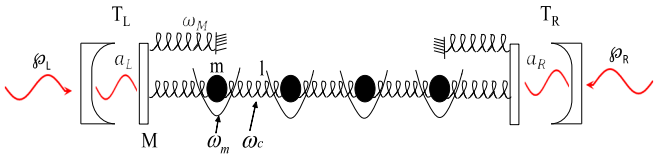

FIG. 1. A particle chain connected to two cavity-optomechanical systems at two ends. The left and right cavity-optomechanical systems are driven by two lasers with power $\wp_L$ and $\wp_R$, respectively. Each optomechanical system has one mechanical oscillator with mass M, resonance frequency ω_M, and damping rate γ. The N particles in the chain are confined by N identical harmonic potentials of the frequency ω_m. Each particle interacts with its neighboring particle harmonically at a frequency ω_c. The environment temperatures of the two cavity-optomechanical systems are T_L and T_R.

respectively, contact the mechanical oscillator of a cavity-optomechanical system. In the chain, each particle is confined by a harmonic potential of the frequency ω_m and has harmonic interaction of the frequency ω_c with its neighboring particles. The Hamiltonian of the harmonic chain is given by

$$H_{\rm chain} = \sum_{n=1}^{N}\left(\frac{p_n^2}{2m} + \frac{m\omega_m^2}{2}x_n^2\right) + \frac{K_c}{2}\sum_{n=1}^{N-1}(x_{n+1}-x_n)^2, \quad (1)$$

where x_n is the displacement of the nth particle from its equilibrium, l is the equilibrium separation between two neighboring particles, and the chain stiffness $K_c = m\omega_c^2$.

In the left or right cavity-optomechanical system, the cavity of resonant frequency ω_0 and photon leakage rate κ constitutes a mechanical oscillator of mass M at a frequency ω_M, and is driven by a laser of the frequency $\omega_{l,L/R}$ and power $\wp_{L/R}$. Hereafter, the subscripts L and R, respectively, denote the physical quantities belonging to the left and right optomechanical system. The Hamiltonian of the left (right) optomechanical system is [56,57]

$$H_{\rm optL/R} = \hbar a_{L/R}^\dagger a_{L/R}\left(\Delta_{L/R}^0 \mp G x_{L/R}\right) + \frac{p_{L/R}^2}{2M} + \frac{K_M x_{L/R}^2}{2} + i\hbar\varepsilon_{L/R}(a_{L/R}^\dagger - a_{L/R}), \quad (2)$$

where $-$ and $+$ are, respectively, used for the left and right optomechanical systems; $a_{L/R}$ and $a_{L/R}^\dagger$ are the annihilation and creation operators for the left and right cavity field, respectively; $x_L(x_R)$ is the displacement of the left (right) mechanical oscillator from its equilibrium; G is the optomechanical coupling strength; stiffness $K_M = M\omega_M^2$; Δ_L^0 and Δ_R^0 are the detuning of optical frequency from the left and right cavity resonant frequency, given by

$$\Delta_{L/R}^0 = \omega_0 - \omega_{l,L/R}, \quad (3)$$

and $\varepsilon_{L/R} = \sqrt{2\kappa j_{{\rm in}L/R}}$ with the input photon flux on the left and right optomechanical system $j_{{\rm in}L/R} = \wp_{L/R}/(\hbar\omega_{l,L/R})$.

The far-left particle and the far-right particle interact with the left and right cavity-optomechanical system harmonically and the interaction Hamiltonian is

$$H_{\rm int} = \tfrac{1}{2}K_{\rm in}[(x_1 - x_L)^2 + (x_R - x_N)^2], \quad (4)$$

in which $K_{\rm in}$ is the stiffness of the interaction force between the particle and the mechanical oscillator.

The total Hamiltonian of the hybrid system is $H_{\rm tot} = H_{optL} + H_{optR} + H_{\rm chain} + H_{\rm int}$. Now we introduce dimensionless positions and momentums,

$$Q_{L/R} = \sqrt{M\omega_M/\hbar}x_{L/R}, \quad P_{L/R} = p_{L/R}/\sqrt{M\hbar\omega_M}, \quad (5)$$

and

$$Q_n = \sqrt{(m\omega_c)/\hbar}x_n, \quad P_n = p_n/\sqrt{m\hbar\omega_c}. \quad (6)$$

The Heisenberg equations of motion for the two cavity-optomechanical systems are governed by

$$\begin{aligned}
\dot{P_L} &= \sqrt{2}g_0 a_L a_L^\dagger + \Omega Q_1 - (1+\varsigma_{_M})\omega_M Q_L - \gamma P_L + \xi_L(t),\\
\dot{P_R} &= -\sqrt{2}g_0 a_R a_R^\dagger + \Omega Q_N - (1+\varsigma_{_M})\omega_M Q_R - \gamma P_R + \xi_R(t),\\
\dot{a_L} &= -\left[i\left(\Delta_L^0 - \sqrt{2}g_0 Q_L\right) + \kappa\right]a_L + \varepsilon_L + \sqrt{2\kappa}a_{inL}(t),\\
\dot{a_R} &= -\left[i\left(\Delta_R^0 + \sqrt{2}g_0 Q_R\right) + \kappa\right]a_R + \varepsilon_R + \sqrt{2\kappa}a_{inR}(t),
\end{aligned} \quad (7)$$

with the vacuum-optomechanical coupling rate $g_0 = \sqrt{\hbar/(2M\omega_M)}G$, the chain-oscillator coupling constant $\alpha = \varsigma_{_M}\varsigma_{_c}$, and $\Omega = \omega_M(\alpha\varkappa)^{1/2}$. Here, the ratios $\varsigma_{_M} = K_{\rm in}/K_M$, $\varsigma_{_c} = K_{\rm in}/K_c$, $\varkappa = \omega_c/\omega_M$ determine the relative strength between the oscillator vibration, particle oscillation, and the particle-oscillator vibration. We introduce the damping of the mechanical oscillator with a rate γ, and vacuum noise a_{inL} and a_{inR} entering the left and right optomechanical system from the drive port, and thermal noise $\xi_L(\xi_R)$ associated with the mechanical damping phenomenally. The correlations for the two noises are given by

$$\langle a_{{\rm in}L/R}(t)a_{{\rm in}L/R}^\dagger(t')\rangle = \delta(t-t'), \quad (8)$$

and $\langle\xi_{L/R}(t)\xi_{L/R}(t')\rangle = \int \eta_{L/R}(\omega)e^{-i\omega(t-t')}d\omega$ with [57,58]

$$\eta_{L/R}(\omega) = \frac{\gamma}{2\pi\omega_M}\omega\left[1 + \coth\left(\frac{\hbar\omega}{2k_B T_{L/R}}\right)\right], \quad (9)$$

and the Boltzmann constant k_B. When the two optomechanical systems are decoupled with the chain ($\alpha = 0$), the effective temperature of each optomechanical system can be controlled by the driving laser [56,57,59–63]. To make the two optomechanical systems function as two reservoirs, α should be kept small so that the temperatures cannot be significantly changed by the coupling to the chain.

The Heisenberg equations of motion for the particles in the chain are

$$\begin{aligned}
\dot{P_1} &= \omega_c[Q_2 - (1+\varsigma_c+\zeta^2)Q_1] + \Omega Q_L,\\
\dot{P_n} &= \omega_c[Q_{n+1} + Q_{n-1} - (2+\zeta^2)Q_n], \quad n = 2,\ldots,N-1,\\
\dot{P_N} &= -\omega_c[(1+\varsigma_c+\zeta^2)Q_N - Q_{N-1}] + \Omega Q_R,
\end{aligned} \quad (10)$$

with the ratio $\zeta = \omega_m/\omega_c$.

Now, to solve the nonlinear Eqs. (7) and (10), we write

$$\begin{aligned}
a_{L/R} &= \alpha_{sL/R} + \delta a_{L/R}, \quad a_{L/R}^\dagger = \alpha_{sL/R}^* + \delta a_{L/R}^\dagger,\\
P_{L/R} &= \langle P_{L/R}\rangle + \delta P_{L/R}, \quad Q_{L/R} = \langle Q_{L/R}\rangle + \delta Q_{L/R},\\
P_n &= \langle P_n\rangle + \delta P_n, \quad Q_n = \langle Q_n\rangle + \delta Q_n,
\end{aligned} \quad (11)$$

where $\langle\hat{A}\rangle$ stands for the expectation value of the operator $\hat{A}$, $\alpha_{sL/R} = \langle a_{L/R}\rangle$; and $\delta a_{L/R}$, $\delta P_{L/R}$, $\delta Q_{L/R}$, δQ_n, and δP_n are the quantum fluctuation of the relevant operator.

A. Expectation values of operators of the hybrid system in steady state

Taking the expectation values of Eqs. (7) and (10) and making the approximation $\langle\widehat{A}\widehat{B}\rangle \approx \langle\widehat{A}\rangle\langle\widehat{B}\rangle$, we get the steady-state equations for the optomechanical system,

$$\begin{aligned}
\sqrt{2}g_0 N_{sL} &= \omega_M(1+\varsigma_M)\langle Q_L\rangle - \Omega\langle Q_1\rangle,\\
\sqrt{2}g_0 N_{sR} &= -\omega_M(1+\varsigma_M)\langle Q_R\rangle + \Omega\langle Q_N\rangle,\\
\langle P_{L/R}\rangle &= 0, \quad N_{sL/R} = \frac{2\kappa j_{\mathrm{in}L/R}}{\Delta_{L/R}^2+\kappa^2},
\end{aligned} \tag{12}$$

with steady-state intercavity photon number $N_{sL/R} = |\alpha_{sL/R}|^2$, and

$$\Delta_{L/R} = \Delta_{L/R}^0 \mp \sqrt{2}g_0\langle Q_{L/R}\rangle. \tag{13}$$

The steady-state equations for the harmonic chain are

$$\begin{aligned}
\tilde{\alpha}\langle Q_L\rangle &= (1+\varsigma_c+\zeta^2)\langle Q_1\rangle - \langle Q_2\rangle,\\
\langle P_n\rangle &= 0,\\
\langle Q_{n+1}\rangle &= (2+\zeta^2)\langle Q_n\rangle - \langle Q_{n-1}\rangle,\ n=2,\ldots,N-1,\\
\tilde{\alpha}\langle Q_R\rangle &= (1+\varsigma_c+\zeta^2)\langle Q_N\rangle - \langle Q_{N-1}\rangle,
\end{aligned} \tag{14}$$

where

$$\tilde{\alpha} = (\alpha/\varkappa)^{1/2}. \tag{15}$$

The detailed process of solving Eqs. (12) and (14) is given in Appendix A.

B. Quantum fluctuation in the hybrid system

From Eqs. (7) and (10), quantum fluctuations $\delta a_{L/R}$, $\delta P_{L/R}$, and δP_n are governed by

$$\begin{aligned}
\delta\dot{P}_L &= \sqrt{2}g_0(\alpha_{sL}^*\delta a_L + \alpha_{sL}\delta a_L^\dagger) + \Omega\delta Q_1\\
&\quad - (1+\varsigma_M)\omega_M\delta Q_L - \gamma\delta P_L + \xi_L(t),\\
\delta\dot{P}_R &= -\sqrt{2}g_0(\alpha_{sR}^*\delta a_R + \alpha_{sR}\delta a_R^\dagger) + \Omega\delta Q_N\\
&\quad - (1+\varsigma_M)\omega_M\delta Q_R - \gamma\delta P_R + \xi_R(t),\\
\delta\dot{a}_L &= -(i\Delta_L+\kappa)\delta a_L + i\sqrt{2}g_0\alpha_{sL}\delta Q_L + \sqrt{2\kappa}a_{inL}(t),\\
\delta\dot{a}_R &= -(i\Delta_R+\kappa)\delta a_R - i\sqrt{2}g_0\alpha_{sR}\delta Q_R + \sqrt{2\kappa}a_{inR}(t),
\end{aligned} \tag{16}$$

$$\begin{aligned}
\delta\dot{P}_1 &= \omega_c[\delta Q_2 - (1+\varsigma_c+\zeta^2)\delta Q_1] + \Omega\delta Q_L,\\
\delta\dot{P}_n &= \omega_c[\delta Q_{n+1} + \delta Q_{n-1} - (2+\zeta^2)\delta Q_n],\\
&\quad n=2,\ldots,N-1,\\
\delta\dot{P}_N &= -\omega_c[(1+\varsigma_c+\zeta^2)\delta Q_N - \delta Q_{N-1}] + \Omega\delta Q_R.
\end{aligned} \tag{17}$$

Performing Fourier transformation on both sides of Eqs. (16) and (17) to the frequency domain by using $f(t) = \int_{-\infty}^{\infty} f(\omega)e^{-i\omega t}d\omega/(2\pi)$ and $f^\dagger(t) = \int_{-\infty}^{\infty} f^\dagger(-\omega)e^{-i\omega t}d\omega/(2\pi)$, we obtain the quantum fluctuations $\delta Q_n(\omega)$ of the nth particle in the frequency domain,

$$\delta Q_n(\omega) = G_L(n,\omega)\delta Q_L(\omega) + G_R(n,\omega)\delta Q_R(\omega). \tag{18}$$

Here, the left and right propagators

$$G_L(n,\omega) = \tilde{\alpha}\frac{B_{N-n+1}(\omega)}{C_N(\omega)},\ G_R(n,\omega) = \tilde{\alpha}\frac{B_n(\omega)}{C_N(\omega)}, \tag{19}$$

with

$$C_N(\omega) = B_{N+1}(\omega) + (\varsigma_c - 1)B_N(\omega), \tag{20}$$

$$B_n(\omega) = \Xi_n(\omega) + (\varsigma_c - 1)\Xi_{n-1}(\omega), \tag{21}$$

$$\Xi_n(\omega) = \begin{cases} \sinh[n\Gamma(\omega)]/\sinh[\Gamma(\omega)] & \text{for } 0<\omega<\Omega_L\\ \sin[n\Gamma(\omega)]/\sin[\Gamma(\omega)] & \text{for } \Omega_L<\omega<\Omega_H\\ (-1)^n\sinh[n\Gamma(\omega)]/\sinh[\Gamma(\omega)] & \text{for } \omega>\Omega_H, \end{cases} \tag{22}$$

$$\Gamma(\omega) = \begin{cases} \ln[\sigma(\omega)+\sqrt{\sigma^2(\omega)-1}] & \text{for } 0<\omega<\Omega_L\\ \arccos\sigma(\omega) & \text{for } \Omega_L<\omega<\Omega_H\\ \ln[-\sigma(\omega)-\sqrt{\sigma^2(\omega)-1}] & \text{for } \omega>\Omega_H, \end{cases} \tag{23}$$

where

$$\sigma(\omega) = 1 + \left(\omega_m^2 - \omega^2\right)/(2\omega_c^2) \tag{24}$$

and

$$\Omega_L = \omega_m, \quad \Omega_H = \omega_m\sqrt{1+4\zeta^{-2}}. \tag{25}$$

$\delta Q_L(\omega)$ and $\delta Q_R(\omega)$ are given by

$$\begin{pmatrix}\delta Q_L(\omega)\\ \delta Q_R(\omega)\end{pmatrix} = \begin{pmatrix} R_L(\omega) & R_C(\omega)\\ R_C(\omega) & R_R(\omega)\end{pmatrix}\begin{pmatrix}\xi_L(\omega)+F_{\mathrm{Lrad}}(\omega)\\ \xi_R(\omega)+F_{\mathrm{Rrad}}(\omega)\end{pmatrix}. \tag{26}$$

The total susceptibility $R_L(\omega)$ $[R_R(\omega)]$ of the left (right) cavity-optomechanical system takes account of the response of the left (right) mechanical oscillator to the total external forces in the left (right) end; the cross susceptibility $R_C(\omega)$ of the left (right) cavity-optomechanical system accounts for the response of the left (right) mechanical oscillator to the total external forces in the right (left) end. $R_L(\omega)$ $[R_R(\omega)]$ and $R_C(\omega)$ are given by

$$R_{L/R}(\omega) = \frac{C_N(\omega) - \alpha B_N(\omega)\omega_M\chi_{R/L}(\omega)}{\chi_{R/L}(\omega)D_N(\omega)\omega_M^2}, \tag{27}$$

$$R_C(\omega) = \frac{\alpha}{D_N(\omega)\omega_M}, \tag{28}$$

with

$$\begin{aligned}
D_N(\omega) &= \frac{C_N(\omega) - \alpha B_N(\omega)\omega_M[\chi_L(\omega)+\chi_R(\omega)]}{\omega_M^2\chi_L(\omega)\chi_R(\omega)}\\
&\quad + \alpha^2\Xi_{N-1}(\omega),
\end{aligned} \tag{29}$$

and the susceptibility $\chi_L(\omega)$ and $\chi_R(\omega)$ of the left and right cavity-optomechanical system is given by

$$\chi_{L/R}^{-1}(\omega) = \frac{\omega_M^2(1+\varsigma_M) - \omega^2 + i\omega\gamma}{\omega_M} + \frac{4\Delta_{L/R}g_0^2 N_{sL/R}}{(\kappa - i\omega)^2 + \Delta_{L/R}^2}. \tag{30}$$

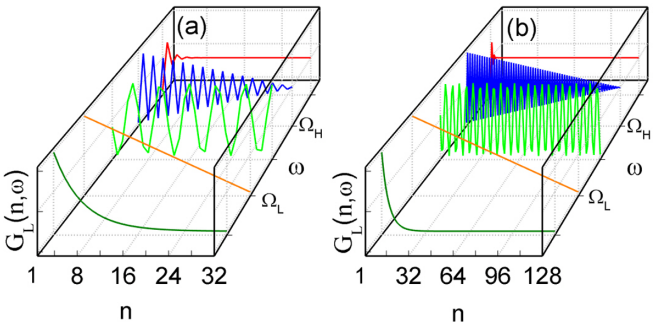

FIG. 2. Left propagator $G_L(n,\omega)$ as a function of n at different frequencies: $\omega < \Omega_L$ (olive), $\omega = \Omega_L$ (orange), $\Omega_L < \omega < \Omega_H$ (green), $\omega = \Omega_H$ (blue), $\omega > \Omega_H$ (red). The particle number (a) $N = 32$ and (b) $N = 128$.

$\xi_{L/R}(\omega)$ are the Fourier spectrums of the stochastic forces induced by Brownian noise, with the correlation function given by

$$\langle \xi_{L/R}(\omega)\xi_{L/R}(\Omega)\rangle = 4\pi^2\eta_{L/R}(\omega)\delta(\omega+\Omega). \tag{31}$$

$F_{L/\mathrm{Rrad}}(\omega)$ are the Fourier spectrums of the stochastic forces generated by the radiation pressure backaction, given by

$$F_{L/\mathrm{Rrad}}(\omega) = \frac{2\sqrt{\kappa}g_0\alpha_{sL/R}a_{\mathrm{in}L/R}(\omega)}{\kappa + i(\Delta_{L/R}-\omega)} + \mathrm{H.c.}, \tag{32}$$

in which the correlation function of the vacuum noise is given by

$$\langle a_{\mathrm{in}L/R}(\omega)a^{\dagger}_{\mathrm{in}L/R}(-\Omega)\rangle = 2\pi\delta(\omega+\Omega). \tag{33}$$

C. Conditions for the effective propagation of the fluctuation of the optomechanical systems along the chain

The thermal fluctuation of a mechanical oscillator of the optomechanical system can excite the lattice vibration modes and can further be propagated from one end to another end via the modes. Thus, the properties of the lattice modes are important for the propagation. Assuming $\delta Q_n(t) = Ae^{i(\mathrm{nql}-\omega t)}$ with the wave vector q of the lattice wave [64,65], from Eq. (17) we obtain the dispersion relation of the particle chain,

$$\omega_k(q_k) = \omega_m\sqrt{1+4\zeta^{-2}\sin^2(q_k l/2)}, \tag{34}$$

where $\omega_k(q_k)$ is the frequency corresponding to the kth lattice vibration mode, and q_k is the corresponding wave vector. Ω_L and Ω_H defined in Eq. (25) are, respectively, the minimum and the maximum frequencies of $\omega_k(q_k)$, indicating the relation of the thermal fluctuation propagation to the lattice waves.

Equation (18) shows that $G_L(n,\omega)$ and $G_R(n,\omega)$ describe the propagation of the fluctuations of the left and right mechanical oscillators from one end to another end. Actually this propagation is limited by the lattice dispersion relation, as studied in Fig. 2, where the site distribution of the left propagator $G_L(n,\omega)$ at different frequencies ω for the chain length $N = 32$ (left) and $= 128$ (right) are shown. The right propagator $G_R(n,\omega)$ is not shown here since it has a similar site distribution. The parameters used in the calculation are listed in Table I and will be used in the following numerical simulations unless otherwise specified. Figure 2 shows that

TABLE I. Optical and mechanical parameters for the hybrid chain-optomechanical system used in the simulation.

K_{in}	M	m	$\omega_m/2\pi$	$\omega_c/2\pi$
6 nN/μm	21 pg	1.1 pg	500 kHz	380 kHz
$\omega_M/2\pi$	$\kappa/2\pi$	κ/ω_M	$g_0/2\pi$	$Q_M = \omega_M/\gamma$
830 kHz	166 kHz	0.2	13 Hz	4×10^4

when $\omega < \Omega_L$ or $\omega > \Omega_H$, $G_L(n,\omega)$ quickly decays with the site n, and especially with the increasing of the lattice length N, the decay rate increases greatly. Thus, the fluctuation of the optomechanical systems at the frequency ω can be effectively propagated from the one end to another end of the chain when ω is within the phonon band ($\Omega_L < \omega < \Omega_H$).

To facilitate the controlling cavity-optomechanical system in a wide range from the quantum ground state to the classical motion, the weak optomechanical coupling ($g_0|\alpha_{sL/R}| \ll \kappa$) and condition of the sideband cooling mechanical oscillator motion ($\Delta_{L/R} = \omega_M$) [56,57,59–63] are assumed in our numerical calculation. In this situation, for a single optomechanical system ($\alpha = 0$), normal-mode splitting does not occur and $R_{L/R}(\omega)$ has a peak at $\omega = \omega_M$ [56]. Further, to make the optomechanical systems function as reservoirs for the chain, a weak coupling between the mechanical oscillator and the chain ($\alpha \ll 1$) is assumed in this paper, so that the peak position of $R_{L/R}(\omega)$ at $\omega = \omega_M$ is nearly unchanged. The interaction between the end particle and the mechanical oscillator could be realized via van der Waals interaction, and thus $\alpha \ll 1$ could be realized.

The effective coupling of the thermal fluctuation by the cavity to the chain requires the cavity vibration frequency ω_M to match the lattice vibration frequency, i.e.,

$$\Omega_L < \omega_M < \Omega_H. \tag{35}$$

The condition (35) is assumed in the following numerical analysis.

III. THERMAL FLUX ALONG THE CHAIN

Using Eqs. (8), (9), and (30), we obtain the mean phonon occupancy at the frequency ω of the left and right cavity-optomechanical heat bath [56,57],

$$n_{L/R}(\omega) = \gamma\frac{n_{L/RT}(\omega) + n_{L/\mathrm{Rrad}}(\omega)}{\gamma_{L/R}(\omega)}, \tag{36}$$

with the mechanical decay rate $\gamma_{L/R}(\omega)$ of the left and right cavity-optomechanical systems,

$$\gamma_{L/R}(\omega) = \gamma\left\{1+\gamma^{-1}\frac{8\Delta_{L/R}\omega_M\kappa g_0^2 N_{sL/R}}{\left(\Delta_{L/R}^2-\kappa^2-\omega^2\right)^2+4\Delta_{L/R}^2\kappa^2}\right\}, \tag{37}$$

and the mean phonon occupancy induced by the environments at the frequency ω,

$$n_{L/RT}(\omega) = \coth[\hbar\omega/(2k_BT_{L/R})]/2, \tag{38}$$

at the environmental temperature $T_{L/R}$, and the thermal phonon occupancy $n_{L/\mathrm{Rrad}}(\omega)$ induced by the radiation pres-

sure backaction,

$$n_{L/\mathrm{Rrad}}(\omega)=\frac{2\omega_M\kappa\left(\kappa^2+\Delta_{L/R}^2+\omega^2\right)g_0^2N_{sL/R}}{\left[\left(\Delta_{L/R}^2-\kappa^2-\omega^2\right)^2+4\Delta_{L/R}^2\kappa^2\right]\omega\gamma}. \quad (39)$$

The difference of the mean phonon occupancy $n_{L/R}(\omega)$ in the left and right optomechanical systems, i.e., $\Delta n(\omega)\equiv n_L(\omega)-n_R(\omega)$, includes two parts: the difference of thermal phonons induced by the environments, $\Delta n_T(\omega)=n_{LT}(\omega)-n_{RT}(\omega)$, and the difference of thermal phonons induced by the radiation pressure backaction, $\Delta n_{rad}(\omega)=n_{\mathrm{Lrad}}(\omega)-n_{\mathrm{Rrad}}(\omega)$. When the environmental temperatures T_L and T_R are different, $\Delta n_T(\omega)\neq 0$; or when the driving powers $\wp_L$ and $\wp_R$ are different, $\Delta n_{rad}(\omega)\neq 0$. In both cases, the difference of the mean phonon occupancy $n_{L/R}(\omega)$ in the left and right optomechanical systems can lead to the heat flux through the chain. The local heat flux through the nth particle is defined as (see Appendix B)

$$J_n(t)=\frac{l\hbar\omega_c^2}{4}[\delta P_{n+1}(t)+\delta P_n(t)][\delta Q_n(t)-\delta Q_{n+1}(t)]+\mathrm{H.c.}, \quad (40)$$

where H.c. stands for Hermitian conjugate. After transient time, the heat flux can reach a steady state. The local heat flux at the steady state can be calculated with the time average of $J_n(t)$, $\langle J_n(t)\rangle=\lim_{T-\infty}\int_0^T J_n(t)dt/T$, where the symbol $\langle\cdot\rangle$ represents the time average. To calculate $\langle J_n(t)\rangle$, we introduce

$$\langle J_n(t,\tau)\rangle=\frac{l\hbar\omega_c^2}{4}\left\langle\begin{matrix}[\delta P_{n+1}(t)+\delta P_n(t)][\delta Q_n(t+\tau)\\ -\delta Q_{n+1}(t+\tau)]+\mathrm{H.c.}\end{matrix}\right\rangle. \quad (41)$$

The calculation of the right side of Eq. (41) can be transformed into the frequency domain with the Wiener-Khinchin theorem [66] using Eqs. (18)–(26) as well as $\delta P_n(\omega)=-i\omega\delta Q_n(\omega)/\omega_c$. Using $\langle J_n(t)\rangle=\langle J_n(t,0)\rangle$, we obtain

$$J_N=\int_{-\infty}^{\infty}\tilde{J}_N(\omega)d\omega,\quad \tilde{J}_N(\omega)=j(\omega)\rho_N(\omega). \quad (42)$$

Here, $\tilde{J}_N(\omega)$ is the thermal flux due to the difference of phonons of the frequency ω between the two cavities, and the maximum heat flux induced by the phonon number difference at the frequency ω between the left and right optomechanical systems is given by

$$j(\omega)=\gamma_e(\omega)\Delta n(\omega)\hbar\omega l/2, \quad (43)$$

where the effective damping rate $\gamma_e(\omega)$ of the cavity-chain system reads

$$\gamma_e(\omega)=\gamma_L(\omega)\gamma_R(\omega)/\overline{\gamma}(\omega), \quad (44)$$

with $\overline{\gamma}(\omega)=[\gamma_L(\omega)+\gamma_R(\omega)]/2$. The propagation efficiencies $\rho_N(\omega)$ read

$$\rho_N(\omega)=\frac{2\alpha^2\omega^2\overline{\gamma}(\omega)}{\pi\omega_M^4|D_N(\omega)|^2}. \quad (45)$$

A. Dependence of $j(\omega)$ on the environmental temperature and driving laser power

$j(\omega)$ is dependent on the environmental temperature and can be controlled by the driving lasers. In Fig. 3, we study $j(\omega)$ in the case that the environmental temperatures ($T_L=2$ K and $T_R=1$ K) in the two cavities are higher than the Debye temperature $\Theta_D\equiv\hbar\Omega_H/k_B$, where the insets in Fig. 3 shows the mean phonon occupancy of the mechanical oscillator of the optomechanical system. For a moderate mechanical quality factor ω_M/γ in Table I, the mean phonon occupancy is much larger than 1 [cf. the inset in Fig. 3(a)]. For the mechanical quality ω_M/γ up to 8×10^6, cooling the mechanical oscillator close to the ground state can be achieved as shown in the inset in Fig. 3(b). In both cases, $j(\omega)$ has a peak or dip around $\omega=\omega_M$. But the the curve of $j(\omega)$ in Fig. 3(b) is nearly flat for $\omega\leqslant\omega_M$, and $j(\omega)$ decays quickly with ω when $\omega>\omega_M$.

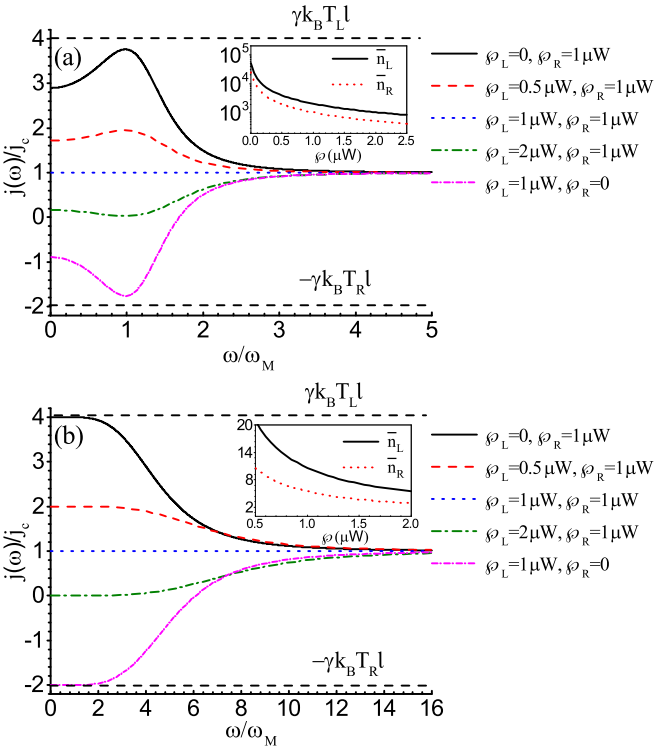

FIG. 3. $j(\omega)$ as a function of ω under different laser drive powers $\wp_L$ and $\wp_R$ at the environmental temperatures $T_L=2$ K and $T_R=1$ K higher than the Debye temperature Θ_D. The inset shows the mean phonon occupancy $\bar{n}_{L/R}$ of the left and right mechanical oscillator of the optomechanical system under the sideband cooling $\Delta_{L/R}=\omega_M$. The quality factor (a) $Q_M=\omega_M/\gamma=4\times10^4$ and (b) $Q_M=\omega_M/\gamma=8\times10^6$.

When the two cavities are driven by the same power, the heat flux is induced by the difference of environmental temperatures. When the driving laser powers in the two cavities are not equal, the maximum heat flux $j(\omega)$ can be tuned by the difference of the laser powers. Figure 3 shows that even the direction of the heat flux can be tuned. Using $n_{L/RT}(\omega)=k_BT_{L/R}/\hbar\omega$ in Eq. (43), and ignoring the weak mean phonon occupancy induced by the radiation pressure backaction, we get that $j(\omega)$ in the high-temperature regime is approximated by

$$j(\omega)=j_c\Delta T_e(\omega)/\Delta T, \quad (46)$$

where $\Delta T=T_L-T_R$ is the environmental temperature difference,

$$j_c=\gamma k_B\Delta T l/2 \quad (47)$$

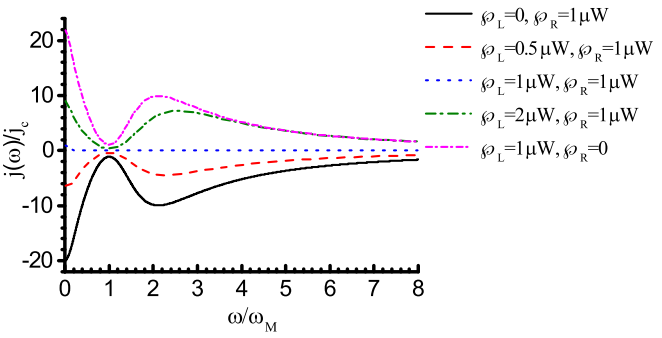

FIG. 4. $j(\omega)$ as a function of ω under different laser drive powers $\wp_L$ and $\wp_R$ at the environment temperatures $T_L = 0.25\Theta_D$ and $T_R = 0.15\Theta_D$.

is the classical local heat flux of the harmonic chain for $\gamma \ll \omega_c$ without the laser driving [22], and

$$\Delta T_e(\omega) = T_{eL}(\omega) - T_{eR}(\omega), \tag{48}$$

with the effective temperature $T_{eL/R}(\omega)$ of the left and right cavity-optomechanical heat bath at ω, given by

$$T_{eL/R}(\omega) = T_{L/R}\gamma_{R/L}(\omega)/\overline{\gamma}(\omega). \tag{49}$$

Thus, when the laser power in the high-temperature end is much stronger than that in the low-temperature end so that $\gamma_L(\omega)/\gamma_R(\omega) \gg 1$, $\Delta T_e(\omega)/\Delta T < 0$, the direction of the heat flux can be reversed, as shown in Fig. 3. However, there is a upper limit for the heat flux. When $\wp_L \ll \wp_R$, $\gamma_L(\omega) \ll \gamma_R(\omega)$, $\Delta T_e(\omega) = 2T_L$, $j(\omega)$ reaches its maximum $\gamma k_B l T_L$; when $\wp_L \gg \wp_R$, $\gamma_L(\omega) \gg \gamma_R(\omega)$, $\Delta T_e(\omega) = -2T_R$, $j(\omega)$ reaches its minimum $-\gamma k_B l T_R$.

In Fig. 4, we study $j(\omega)$ in the case that the environmental temperatures in the two cavities are lower than the Debye temperature Θ_D such that $n_{L/RT} \ll n_{L/\mathrm{Rrad}}$. This case is dramatically different from that in Fig. 3, i.e., $j(\omega) \approx 0$ now at $\omega = \omega_M$. In this situation, $n_{L/\mathrm{Rrad}} \approx \kappa^2/(4\omega_M^2) + 1/2$ at ω_M, $j(\omega) \approx \Delta n_{rad} \approx 0$.

$j(\omega)$ for $T_L = T_R$ has similar features demonstrated in Figs. 3 and 4, and thus is not shown here.

B. Frequency distribution of ρ_N on the mechanical properties of the system

Propagation efficiency $\rho_N(\omega)$ is dependent on the mechanical properties of the system. Figure 5 shows the frequency distribution of propagation efficiency $\rho_N(\omega)$ for different chain lengths characterized by the particle number N. Due to weak optomechanical coupling ($g_0|\alpha_{sL/R}| \ll \kappa$) and weak mechanical coupling ($\alpha << 1$), $\rho_N(\omega)$ has a maximum value near $\omega = \omega_M$, and when ω is offset from ω_M, $\rho_N(\omega)$ quickly decays. Except for the major peak around $\omega = \omega_M$, there are many minor peaks. These minor peaks arise from the resonance with the lattice vibration modes, and thus they get dense with the increasing of N. Moreover, as N increases, the propagation efficiency $\rho_N(\omega)$ is essentially nonzero for the frequency interval from Ω_L to Ω_H. This agrees with the frequency distribution of the propagator shown in Fig. 2, where it shows that when $\omega < \Omega_L$ and $\omega > \Omega_H$, the propagation of

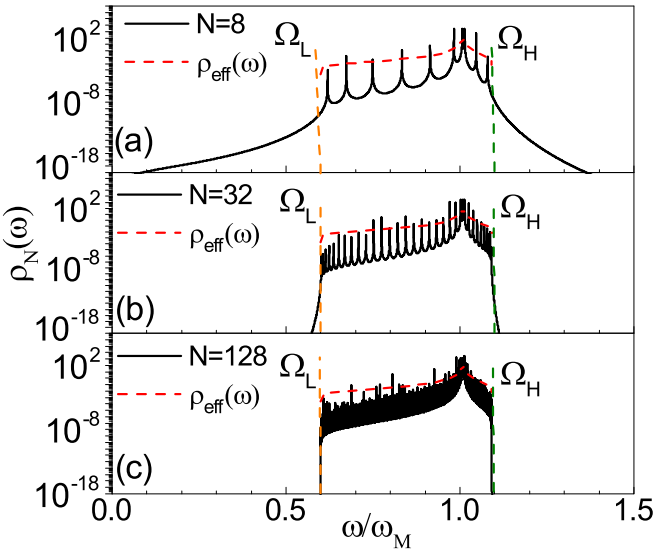

FIG. 5. The propagation efficiency $\rho_N(\omega)$ as a function of ω with different N; $\rho_{\mathrm{eff}}(\omega)$ is also given for comparison. $\wp_L = 1\ \mu\mathrm{W}, \wp_R = 2\ \mu\mathrm{W}$ are used.

the phonons is restricted due to the mismatch of the frequency to the chain mode frequency distribution.

C. Breakdown of the Fourier's law in the harmonic chain

When $N \to \infty$, we divide the integration in Eq. (42) into infinite integrands, each of which contains a peak of $\rho_N(\omega)$. Further, using the properties of $\rho_N(\omega)$ demonstrated in Fig. 5, we obtain

$$J_\infty = 2\int_{\Omega_L}^{\Omega_H} j(\omega)\rho_{\mathrm{eff}}(\omega)d\omega, \tag{50}$$

where the equivalent propagation efficiency

$$\rho_{\mathrm{eff}}(\omega) = \frac{2\alpha\omega\overline{\gamma}(\omega)\sin\Gamma(\omega)}{\pi[\gamma_L(\omega)t_R(\omega) + \gamma_R(\omega)t_L(\omega)]}, \tag{51}$$

with

$$t_{L/R}(\omega) = \left|\frac{\varsigma_c - 2\sin^2[\Gamma(\omega)/2]}{\chi_{L/R}(\omega)} - \alpha\omega_M\right|^2 + \frac{\sin^2\Gamma(\omega)}{|\chi_{L/R}(\omega)|^2}. \tag{52}$$

$\rho_{\mathrm{eff}}(\omega)$ versus ω is plotted in Figs. 5(a)–5(c) to make a comparison of $\rho_{\mathrm{eff}}(\omega)$ with $\rho_N(\omega)$. Figure 5 shows that when N is sufficiently large, the envelope of $\rho_N(\omega)$ is close to $\rho_{\mathrm{eff}}(\omega)$. Moreover, the propagation efficiency is highest at $\omega = \omega_M$, and when ω is off from ω_M, $\rho_{\mathrm{eff}}(\omega)$ quickly decreases.

In Figs. 6 and 7, we investigate J_N and J_∞ in detail using the parameters in Table I except for γ. Figure 6, plotting J_N versus N, shows that when N increases, J_N approaches a finite value J_∞ given by Eq. (50). The finite J_∞ shows that the thermal conductivity of the system is divergent, and thus the Fourier's law does not hold in our system, in agreement with the result on the thermal conduction in a one-dimensional harmonic chain [22–25,28].

In Fig. 6(a), $\gamma/\omega_M = 10^{-2}$, and in Fig. 6(b), $\gamma/\omega_M = 10^{-7}$. Figure 6 shows that γ has an important influence on

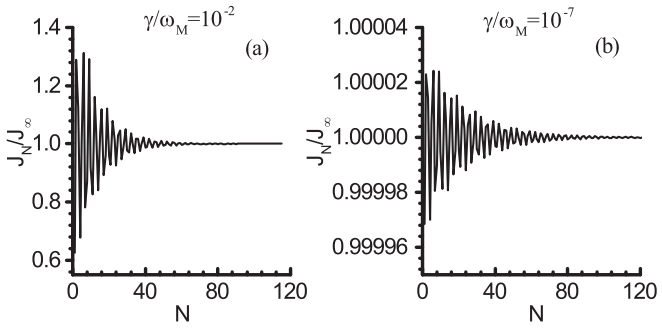

FIG. 6. Heat flux J_N scaled with J_∞ as a function of N obtained with $\wp_L = 1\ \mu$W and $\wp_R = 2\ \mu$W at $T_L = 2$ K, $T_R = 1$ K with (a) $\gamma/\omega_M = 10^{-2}$ and (b) $\gamma/\omega_M = 10^{-7}$.

the velocity of J_N approaching J_∞. In Fig. 7, we plot the heat flux J_N and J_∞ as a function of γ. When the mechanical quality factor $\omega_M/\gamma > 10^3$ or <0.1, using a few number of particles, $J_N \approx J_\infty$; however, the value of the heat flux is greatly reduced. When γ is small, the thermal fluctuation is reduced [cf. Eq. (9)] and thus the particle motion in the chain is little influenced, and even the number of particles is not high to get $J_N \approx J_\infty$. In this situation, J_N and J_∞ are linearly proportional to γ. On the other hand, when the damping rate γ is very high, the mechanical oscillator vibration is reduced and the influence on the particle motion is weak, and thus the heat flux inversely proportional to γ is reduced. Between the two limits, there exists a value of the γ at which the heat flux takes its maximum value, agreeing with the previous result on the thermal conduction in a one-dimensional harmonic chain [22,24].

D. The influence of environmental temperature on the heat flux

Figures 3 and 4 shows that the environmental temperatures have a strong influence on the heat flux. Therefore, using Eq. (36) and $\coth(x) = 1 + 2/(e^{2x} - 1)$, we rewrite Eq. (42) as

$$J_N = J_N^1 + J_N^0, \tag{53}$$

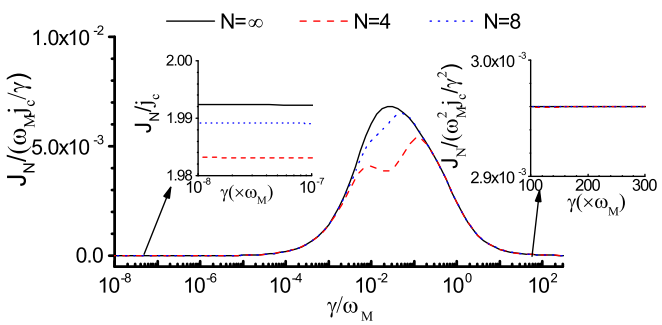

FIG. 7. Heat flux J_N as a function of γ obtained with $\wp_L = 1\ \mu$W and $\wp_R = 2\ \mu$W at $T_L = 2$ K, $T_R = 1$ K. The insets show the relations of the heat flux J_N to very small γ (left) and to large γ (right).

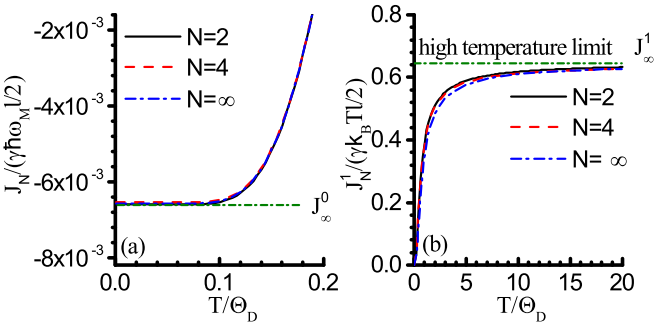

FIG. 8. (a) J_N as a function of T with different N at $T_L = T_R = T$, with T much lower than the Debye temperature Θ_D, and the horizontal line is the heat flux J_∞^0 given by Eq. (55) with $N \to \infty$. (b) J_N^1 as a function of T with different N at $T_L = T_R = T$, and the horizontal line is the heat flux J_∞^1 in the high-temperature limit given by Eq. (56) with $N \to \infty$.

where

$$J_N^1 = \frac{\hbar\gamma l}{2}\int_{-\infty}^{\infty} \frac{\tilde{n}_{LT}(\omega)\gamma_R(\omega) - \tilde{n}_{RT}(\omega)\gamma_L(\omega)}{\overline{\gamma}(\omega)}\omega\rho_N(\omega)d\omega, \tag{54}$$

$$J_N^0 = \frac{\hbar\gamma l}{2}\int_{-\infty}^{\infty} \frac{\Delta\gamma(\omega)}{\overline{\gamma}(\omega)}\frac{\kappa^2 + (\omega - \omega_M)^2}{4\omega_M}\rho_N(\omega)d\omega, \tag{55}$$

with $\Delta\gamma(\omega) = \gamma_L(\omega) - \gamma_R(\omega)$ and $\tilde{n}_{L/RT}(\omega) = [\exp(\hbar\omega/k_B T_{L/R}) - 1]^{-1}$. Here, J_N^1 arises from the thermal phonons of the mechanical oscillator, while J_N^0 comes from the shot-noise fluctuation and is therefore irrelevant to the temperature. When $\kappa \ll \omega_M$, which is used for resolved sideband cooling, J_N^0 is much smaller than J_N^1 in general. However, when $T_{L/R}$ is very low $[\hbar\omega/(2k_B T_{L/R}) \to \infty]$, $\tilde{n}_{L/RT}(\omega)$ is very small and, in this case, J_N^0 cannot be ignored. Figure 8(a), plotting the relation of J_N to the environmental temperature for the case $T_L = T_R = T$, shows that when the temperature is much smaller than the Debye temperature, J_N^0 is dominant; however, when the environmental temperature increases, J_N^1 increases quickly and takes over J_N^0. Figure 8(b) plots the relation of J_N^1 to the environmental temperature for the case $T_L = T_R = T$, and shows that when the temperature is much higher than the Debye temperature, J_N^1 approaches the high-temperature limit, which corresponds to the classical heat flux.

The classical heat flux can be obtained in the following way. We note that ρ_N has a narrow major peak around $\omega = \omega_M$ and around ω_M $j(\omega)$ varies slowly (cf. Fig. 3). Thus, replacing $j(\omega)$ with $j(\omega_M)$ in Eq. (42), we get an approximation,

$$J_N \approx \frac{\gamma k_B \Delta T_e(\omega_M) l}{2}\int_{-\infty}^{\infty}\rho_N(\omega)d\omega, \tag{56}$$

which means that the classical heat flux is proportional to the effective temperature difference at ω_M. Without laser drives, $\Delta T_e(\omega) = \Delta T$, Eq. (56) is accurate and can give the results in Refs. [22,24] on classical thermal conduction in a harmonic chain.

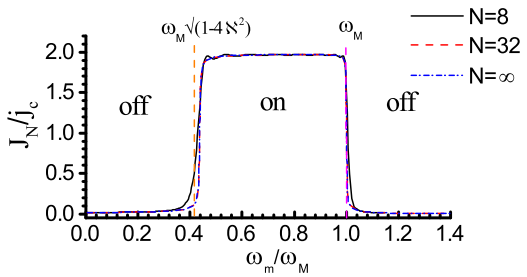

FIG. 9. Heat flux as a function of ω_m for different N at laser drive $\wp_L = 1\ \mu$W, $\wp_R = 2\ \mu$W with $T_L = 2$ K and $T_R = 1$ K.

E. Switching of heat flux

The oscillation frequency of the mechanical oscillator is required to match the lattice wave, i.e., $\Omega_L \lesssim \omega_M \lesssim \Omega_H$, or, equivalently, according to Eq. (25), $\omega_M^2(1-4\varkappa^2) \lesssim \omega_m^2 \lesssim \omega_M^2$. Thus the heat flux can be effectively generated for $\omega_M\sqrt{1-4\varkappa^2} < \omega_m < \omega_M$. This analysis is confirmed by Fig. 9 where J_N versus ω_m is plotted with the ω_M and ω_c in Table I. More interesting, Fig. 9 shows that the heat flux could be switched on or off by controlling the confinement frequency; in particular, the heat flux at $\omega_m \sim \omega_M$ has a sharp transition from on-state of the heat flux to off-state. This property could be used for the thermal switch. This switching effect arises from the fact demonstrated in Fig. 2 that for a long chain, the heat flux cannot be propagated when the frequency cannot match the lattice vibration modes.

IV. MEASURING HEAT FLUX BY THE DIFFERENCE BETWEEN THE CROSS CORRELATIONS OF THE DISPLACEMENTS OF THE LEFT AND RIGHT MECHANICAL OSCILLATORS

In general, it is difficult to directly measure the heat flux in a chain. In this section, noting that the heat flux flowing from one end to other end can generate a correlation of the motion of the two mechanical oscillators, we propose to use this correlation to get information regarding the heat flux. We introduce the difference between the cross correlations between δx_L and δx_R,

$$C_x(\tau) = \langle \delta x_R(t+\tau)\delta x_L(t) + \delta x_L(t)\delta x_R(t+\tau)\rangle - \langle \delta x_L(t+\tau)\delta x_R(t) + \delta x_R(t)\delta x_L(t+\tau)\rangle, \quad (57)$$

and we have

$$\frac{dC_x(\tau)}{d\tau} = \frac{1}{M}F(-\tau), \quad (58)$$

with the difference between the cross correlations between the position and momentum of the two mechanical oscillators,

$$F(\tau) = \langle \delta p_R(t)\delta x_L(t+\tau) + \delta x_L(t+\tau)\delta p_R(t)\rangle - \langle \delta p_L(t)\delta x_R(t+\tau) + \delta x_R(t+\tau)\delta p_L(t)\rangle. \quad (59)$$

Introducing the Fourier transform of $C_x(\tau)$ and $F(\tau)$, i.e., $C_x(\tau) = \int_{-\infty}^{\infty}\tilde{C}_x(\omega)e^{-i\omega\tau}d\omega/(2\pi)$, $F(\tau) = \int_{-\infty}^{\infty}\tilde{F}(\omega)e^{-i\omega\tau}d\omega/(2\pi)$, from Eq. (58) we have

$$\tilde{F}(\omega) = i\omega M\tilde{C}_x(-\omega). \quad (60)$$

When we transform the calculation of the right side of Eq. (59) into the frequency domain, we obtain

$$\tilde{F}(\omega) = \frac{4\pi}{\alpha\omega_M^2}\tilde{J}_N(\omega)C_N(\omega). \quad (61)$$

Comparing Eq. (61) and Eq. (60), we have

$$\tilde{J}_N(\omega) = i\frac{\alpha M\omega_M^2}{4\pi C_N(\omega)}\omega\tilde{C}_x(-\omega). \quad (62)$$

Using Eqs. (62) and (42), we have

$$j(\omega) = i\frac{\alpha M\omega_M^2}{4\pi C_N(\omega)\rho_N(\omega)}\omega\tilde{C}_x(-\omega). \quad (63)$$

Equation (63) shows that once $\tilde{C}_x(-\omega)$ is obtained, the features of $j(\omega)$ in high-temperature and low-temperature regimes, demonstrated in Figs. 3 and 4, can be investigated experimentally.

Further comparing Eq. (42) with Eq. (62), we obtain

$$J_N = \frac{\alpha l M\omega_M^2}{2}\int_{-\infty}^{\infty}C_x(\tau)K_N(\tau)d\tau \quad (64)$$

with

$$K_N(\tau) = \frac{1}{\pi}\int_0^{\infty}\omega\sin(\omega\tau)C_N^{-1}(\omega)d\omega. \quad (65)$$

Equation (64) shows that steady-state heat flux could be obtained from the measurement of the correlation of motion of the two mechanical oscillators.

Our scheme for measuring the thermal flux is similar to that used in Refs. [21,55], where the mean heat flux between two membranes or two particles has been measured and our theoretical analysis could be readily extended to those cases. References [21,55] have shown that this measurement method has a capability to measure the weak thermal flux. For example, a weak thermal flux as weak as $10^{-17}l$ J/s [67] has been measured [21], and even weaker thermal flux could be measured [68] using this method.

V. CONCLUSION

We have investigated thermal conduction in a chain of identical particles connected with two identical optomechanical systems in contact with an independent thermal bath at different temperatures. We find that the thermal conductivity of our system diverges as the number of particles increases, and thus Fourier's law does not hold. As the environment temperature decreases, this system exhibits a transition from classical thermal conduction to quantum thermal conduction, and the heat flux tends to a constant when the environment temperature is much lower than the Debye temperature. Moreover, by controlling the on-site confinement frequency, the heat flux can be switched on or off, offering an approach to the heat switch or thermal transistor [41,42]. Finally, we propose a scheme to measure the heat flux by measuring the difference between the cross correlations of the displacements of the left and right mechanical oscillators.

Using current techniques of manipulating particles [69–79], our harmonic model can be experimentally realized. The particles in the chain can be ions, or charged or neutral nanospheres. For the charged particles, there is the Coulomb

interaction between them [48–54]. For neutral particles, the optical binding potential between optically levitated particles [76–80] can be introduced. N identical on-site harmonic potentials can be provided by N identical optical tweezers [80,81]. When the on-site potential is sufficiently strong, the trapped particles oscillate in their own equilibrium positions, such that the interaction between neighboring particles can be approximated by the harmonic potential. Furthermore, when these constraints are relaxed, our current work can be extended to more complicated cases. For example, when the on-site harmonic potential in the current work is replaced with the cosine potential, which could be realized by two counterpropagating optical fields, the Frenkel-Kontorova model [82] could be realized; in particular, thermal pumping and resonance in driven Frenkel-Kontorova lattices [83] could be studied with cavity-optomechanical systems. Moreover, by setting the random mass of the particles or random on-site potential frequency, thermal conduction in disordered chains [84–86] with cavity-optomechanical systems could be investigated. Finally, by introducing the anharmonic interaction between the particles, our system could be extended to study thermal conduction in anharmonic chains [26,27,30,35,36].

ACKNOWLEDGMENTS

The authors acknowledge support from the Shanghai Municipal Education Commission (Grant No. 2019-01-07-00-05-E00079), National Natural Science Foundation of China (Grants No. 11574085, No. 11834003, No. 91536218), National Key Research and Development Program of China (Grant No. 2017YFA0304201), and Overseas Expertise Introduction Project for Discipline Innovation (Grant No. B12024). The authors thank Dr. J. Millen of King's College London and Prof. Sheng Jiteng, Prof. Li Baowen, Prof. He Dahai, and Prof. Wu Haibin for useful discussions and suggestions.

APPENDIX A: CALCULATIONS OF THE EXPECTATION VALUES OF OPERATORS IN STEADY STATE

In order to obtain the expectation value of the cavity-optomechanical system in the steady state from Eq. (12), we need to solve $\langle Q_1\rangle$ and $\langle Q_N\rangle$ first. Solving Eq. (14), we get

$$\begin{aligned}\langle Q_1\rangle &= \tilde{\alpha}\frac{A_N\langle Q_L\rangle + \langle Q_R\rangle}{A_N^2-1}S_N,\\ \langle Q_N\rangle &= \tilde{\alpha}\frac{\langle Q_L\rangle + A_N\langle Q_R\rangle}{A_N^2-1}S_N,\\ \langle Q_n\rangle &= \frac{S_{N-n+1}\langle Q_1\rangle + S_n\langle Q_N\rangle}{S_N},\end{aligned} \tag{A1}$$

with

$$S_n = \frac{s_+^{n-1}-s_-^{n-1}}{s_+-s_-},\ s_\pm = 1+\frac{\zeta^2}{2}\pm\frac{\zeta}{2}\sqrt{\zeta^2+4}, \tag{A2}$$

and

$$A_N = S_{N+1} + (\varsigma_c - 1)S_N. \tag{A3}$$

Substituting Eq. (A1) into Eq. (12), we obtain

$$\langle Q_L\rangle = \frac{\sqrt{2}g_0}{\omega_M}(M_N N_{sL} - L_N N_{sR}), \tag{A4}$$

$$\langle Q_R\rangle = \frac{\sqrt{2}g_0}{\omega_M}(L_N N_{sL} - M_N N_{sR}), \tag{A5}$$

where

$$\begin{aligned}M_N &= \frac{(1+\varsigma_M)O_N - \alpha A_N}{(1+\varsigma_M)^2 O_N - 2\alpha(1+\varsigma_M)A_N + \alpha^2 S_N},\\ L_N &= \frac{\alpha}{(1+\varsigma_M)^2 O_N - 2\alpha(1+\varsigma_M)A_N + \alpha^2 S_N},\\ O_N &= A_{N+1} + (\varsigma_c - 1)A_N.\end{aligned} \tag{A6}$$

Using Eqs. (12), (A4), and (A5), we obtain the steady-state intercavity photon number $N_{sL/R}$.

APPENDIX B: FORMULA FOR THE QUANTUM LOCAL HEAT FLUX

We extend the classical definition of heat flux in Ref. [22] to the quantum case. The heat flux $j(x,t)$ at time t in the position x is defined by the continuity equation,

$$\frac{dh(x,t)}{dt} + \frac{\partial j(x,t)}{\partial x} = 0, \tag{B1}$$

where $h(x,t)$ is the energy density. For a one-dimensional (1D) particle chain, we can write the energy density as the sum of the isolated contributions located in the instantaneous position of each particle [22],

$$h(x,t) = \sum_n h_n(t)\delta(x-x_n), \tag{B2}$$

where $\delta(x)$ is the Dirac distribution function, and

$$h_n = \frac{p_n^2}{2m} + U(x_n) + \frac{1}{2}[V(x_{n+1}-x_n) + V(x_n - x_{n-1})] \tag{B3}$$

is the energy of the nth particle. Here, $U(x_n)$ is the on-site potential and the last term amounts to half of the potential energy of the interactions between the neighboring particles [22]. Similar to Eq. (B2), we can write the heat flux as the sum of the local heat flux,

$$j(x,t) = \sum_n J(x,t)\delta(x-x_n). \tag{B4}$$

Inserting Eq. (B2) and (B4) into Eq. (B1), and using $\frac{\partial J(x,t)}{\partial x}|_{x=x_n} = [J(x_n,t) - J(x_{n-1},t)]/l$, we have

$$\frac{dh_n}{dt} + \frac{J_n - J_{n-1}}{l} = 0, \tag{B5}$$

where J_n denotes $J(x_n,t)$. Equation (B5) is the same as that in classical thermal conductivity theory [22]. In classical theory, dh_n/dt can be directly calculated from Eq. (B3). However, now we have to employ the Heisenberg equation of motion for h_n, $dh_n/dt = [h_n, H_{\text{chain}}]/i\hbar$, to obtain

$$\begin{aligned}\frac{dh_n}{dt} = -\frac{1}{4m}&[(p_{n+1}+p_n)F(x_{n+1}-x_n)\\ &- (p_n + p_{n-1})F(x_n - x_{n-1}) + \text{H.c.}],\end{aligned} \tag{B6}$$

where $F(x) = -dV(x)/dx$ and H.c. stands for the Hermitian conjugate. Comparing Eqs. (B5) and (B6), we obtain the local heat flux given by

$$J_n \equiv \frac{l}{4m}(p_{n+1} + p_n)F(x_{n+1} - x_n) + \text{H.c.} \tag{B7}$$

When ignoring the noncommutative relation between p_n and x_n, Eq. (B7) is reduced to the classical local heat flux in Ref. [22].

For the 1D harmonic chain $[F(x) = -m\omega_c^2 x]$, from Eq. (B7) we have

$$J_n = \frac{\omega_c^2 l}{4}(p_{n+1} + p_n)(x_n - x_{n+1}) + \text{H.c.} \tag{B8}$$

Using the dimensionless positions Q_n and momentums P_n, we get

$$J_n = \frac{\hbar\omega_c^2 l}{4}(P_{n+1} + P_n)(Q_n - Q_{n+1}) + \text{H.c.} \tag{B9}$$

Using $P_n = \langle P_n\rangle + \delta P_n$, $Q_n = \langle Q_n\rangle + \delta Q_n$, $\langle P_n\rangle = 0$, we further have

$$J_n(t) = \frac{\hbar\omega_c^2 l}{4}(\delta P_{n+1} + \delta P_n)(\delta Q_n - \delta Q_{n+1}) + \text{H.c.}, \tag{B10}$$

which is the formula for the local heat flux used in the main text. In deducing Eq. (B10), we have discarded the term $\widetilde{J}_n(t) = \hbar\omega_c^2 l(\delta P_{n+1} + \delta P_n)(\langle Q_n\rangle - \langle Q_{n+1}\rangle)/4 + \text{H.c.}$, which does not affect the steady-state local heat flux since $\langle\widetilde{J}_n(t)\rangle = 0$.

[1] W. Marshall, C. Simon, R. Penrose, and D. Bouwmeester, Phys. Rev. Lett. **91**, 130401 (2003).
[2] B. Pepper, R. Ghobadi, E. Jeffrey, C. Simon, and D. Bouwmeester, Phys. Rev. Lett. **109**, 023601 (2012).
[3] O. Romero-Isart, A. C. Pflanzer, F. Blaser, R. Kaltenbaek, N. Kiesel, M. Aspelmeyer, and J. I. Cirac, Phys. Rev. Lett. **107**, 020405 (2011).
[4] G. Anetsberger, E. Gavartin, O. Arcizet, Q. P. Unterreithmeier, E. M. Weig, M. L. Gorodetsky, J. P. Kotthaus, and T. J. Kippenberg, Phys. Rev. A **82**, 061804(R) (2010).
[5] J. D. Teufel, T. Donner, M. A. Castellanos-Beltran, J. W. Harlow, and K. W. Lehnert, Nat. Nanotechnol. **4**, 820 (2009).
[6] A. G. Krause, M. Winger, T. D. Blasius, Q. Lin, and O. Painter, Nat. Photon. **6**, 768 (2012).
[7] F. G. Cervantes, L. Kumanchik, J. Pratt, and J. Taylor, Appl. Phys. Lett. **104**, 221111 (2014).
[8] S. Forstner, S. Prams, J. Knittel, E. D. vanOoijen, J. D. Swaim, G. I. Harris, A. Szorkovszky, W. P. Bowen, and H. Rubinsztein-Dunlop, Phys. Rev. Lett. **108**, 120801 (2012).
[9] S. Forstner, J. Knittel, E. Sheridan, J. D. Swaim, H. Rubinsztein-Dunlop, and W. P. Bowen, Photon. Sens. **2**, 259 (2012).
[10] D. M. Weld, J. Xia, B. Cabrera, and A. Kapitulnik, Phys. Rev. D **77**, 062006 (2008).
[11] A. A. Geraci, S. J. Smullin, D. M. Weld, J. Chiaverini, and A. Kapitulnik, Phys. Rev. D **78**, 022002 (2008).
[12] C. M. Caves, Phys. Rev. D **23**, 1693 (1981).
[13] U. B. Hoff, G. I. Harris, L. S. Madsen, H. Kerdoncuff, M. Lassen, B. M. Nielsen, W. P. Bowen, and U. L. Andersen, Opt. Lett. **38**, 1413 (2013).
[14] X. Xu and J. M. Taylor, Phys. Rev. A **90**, 043848 (2014).
[15] M. Metcalfe, Appl. Phys. Rev. **1**, 031105 (2014).
[16] Ky. Zhang, F. Bariani, and P. Meystre, Phys. Rev. Lett. **112**, 150602 (2014).
[17] A. Dechant, N. Kiesel, and E. Lutz, Phys. Rev. Lett. **114**, 183602 (2015).
[18] Y. Dong, K. Y. Zhang, F. Bariani, and P. Meystre, Phys. Rev. A **92**, 033854 (2015).
[19] K. Y. Zhang, F. Bariani, and P. Meystre, Phys. Rev. A **90**, 023819 (2014).
[20] A. Xuereb, A. Imparato, and A. Dantan, New J. Phys. **17**, 055013 (2015).
[21] C. Yang, X. R. Wei, J. T. Sheng, and H. B. Wu, Nat. Commun. **11**, 4656 (2020).
[22] S. Lepri, R. Livi, and A. Politi, Phys. Rep. **377**, 1 (2003).
[23] A. Dhar, Adv. Phys. **57**, 457 (2008).
[24] Z. Rieder, J. L. Lebowitz, and E. Lieb, J. Math. Phys. **8**, 1073 (1967).
[25] U. Zurcher and P. Talkner, Phys. Rev. A **42**, 3278 (1990).
[26] S. Lepri, R. Livi, and A. Politi, Phys. Rev. Lett. **78**, 1896 (1997).
[27] K. Aoki, and D. Kusnezov, Phys. Rev. Lett. **86**, 4029 (2001).
[28] A. V. Savin and O. V. Gendelman, Phys. Rev. E **67**, 041205 (2003).
[29] P. Cipriani, S. Denisov, and A. Politi, Phys. Rev. Lett. **94**, 244301 (2005).
[30] T. Mai, A. Dhar, and O. Narayan, Phys. Rev. Lett. **98**, 184301 (2007).
[31] A. Gerschenfeld, B. Derrida, and J. L. Lebowitz, J. Stat. Phys. **141**, 757 (2010).
[32] H. van Beijeren, Phys. Rev. Lett. **108**, 180601 (2012).
[33] L. Delfini, S. Lepri, R. Livi, and A. Politi, Phys. Rev. E **73**, 060201(R) (2006).
[34] A. Dhar, Phys. Rev. Lett. **86**, 3554 (2001).
[35] D. X. Xiong, J. Wang, Y. Zhang, and H. Zhao, Phys. Rev. E **85**, 020102(R) (2012).
[36] D. X. Xiong, Europhys. Lett. **113**, 14002 (2016).
[37] C. W. Chang, D. Okawa, H. Garcia, A. Majumdar, and A. Zettl, Phys. Rev. Lett. **101**, 075903 (2008).
[38] M. Terraneo, M. Peyrard, and G. Casati, Phys. Rev. Lett. **88**, 094302 (2002).
[39] B. W. Li, L. Wang, and G. Casati, Phys. Rev. Lett. **93**, 184301 (2004).
[40] B. Li, J. H. Lan, and L. Wang, Phys. Rev. Lett. **95**, 104302 (2005).
[41] W. C. Lo, L. Wang, and B. W. Li, J. Phys. Soc. Jpn. **77**, 054402 (2008).
[42] B. W. Li, L. Wang, and G. Casati, Appl. Phys. Lett. **88**, 143501 (2006).
[43] L. Wang and B. W. Li, Phys. Rev. Lett. **99**, 177208 (2007).
[44] L. Wang and B. W. Li, Phys. Rev. Lett. **101**, 267203 (2008).

[45] C. W. Chang, D. Okawa, A. Majumdar, and A. Zettl, Science **314**, 1121 (2006).
[46] J. Hwang, M. Pototschnig, R. Lettow, G. Zumofen, A. Renn, S. Götzinger, and V. Sandoghdar, Nature (London) **460**, 76 (2009).
[47] N. B. Li, J. Ren, L. Wang, G. Zhang, P. Hänggi, B. W. Li, Rev. Mod. Phys. **84**, 1045 (2012).
[48] M. Ramm, T. Pruttivarasin, and H. Häffner, New J. Phys. **16**, 063062 (2014).
[49] N. Freitas, E. A. Martinez, and J. P. Paz, Phys. Scr. **91**, 013007 (2016).
[50] M. A. Simón, S. Martínez-Garaot, M. Pons, and J. G. Muga, Phys. Rev. E **100**, 032109 (2019).
[51] A. Ruiz-García, J. J. Fernández, and D. Alonso, Phys. Rev. E **99**, 062105 (2019).
[52] A. Ruiz-García and D. Alonso, Phys. Rev. E **101**, 012129 (2020).
[53] A. Bermudez, M. Bruderer, and M. B. Plenio, Phys. Rev. Lett. **111**, 040601 (2013).
[54] A. Ruiz, D. Alonso, M. B. Plenio, and A. del Campo, Phys. Rev. B **89**, 214305 (2014).
[55] A. Bérut, A. Petrosyan, and S. Ciliberto, Europhys. Lett. **107**, 60004 (2014).
[56] G. S. Agarwal, *Quantum Optics* (Cambridge University Press, New York, 2013).
[57] W. P. Bowen and G. J. Milburn, *Quantum Optomechanics*, (CRC Taylor and Francis Group, Boca Raton, FL, 2016).
[58] U. Zurcher and P. Talkner, Phys. Rev. A **42**, 3267 (1990).
[59] I. Wilson-Rae, N. Nooshi, W. Zwerger, and T. J. Kippenberg, Phys. Rev. Lett. **99**, 093901 (2007).
[60] F. Marquardt, J. P. Chen, A. A. Clerk, and S. M. Girvin, Phys. Rev. Lett. **99**, 093902 (2007).
[61] A. Schliesser, R. Rivière, G. Anetsberger, O. Arcizet, and T. J. Kippenberg, Nat. Phys. **4**, 415 (2008).
[62] A. Schliesser, O. Arcizet, R. Rivière, G. Anetsberger, and T. J. Kippenberg, Nat. Phys. **5**, 509 (2009).
[63] Y. S. Park and H. Wang, Nat. Phys. **5**, 489 (2009).
[64] C. Kittel, *Introduction to Solid State Physics*, (Wiley, New York, 2005).
[65] N. W. Ashcroft and N. D. Mermin, *Solid State Physics* (Harcourt College Publisher, New York, 1976).
[66] L. Cohen, Convolution, filtering, linear systems, the Wiener-Khinchin theorem: Generalizations, in *Proceeding of SPIE*, Advanced Signal Processing Algorithms, Architectures, and Implementations III (SPIE, Bellingham, WA, 1992), Vol. 1770, p. 378.
[67] Sometimes, the particle separation l is dropped in the definition of the thermal flux. In Ref. [21], l is not adopted.
[68] J. Sheng, private communication.
[69] Z. Y. Gong, Y. L. Pan, G. Videen, and C. J. Wang, J. Quantum Spectrosc. Radiat. Transfer **214**, 94 (2018).
[70] Z. He and G. Dong, J. Opt. Soc. Am. B **38**, 60 (2021).
[71] J. Millen, T. S. Monteiro, R. Pettit, and A. N. Vamivakas, Rep. Prog. Phys. **83**, 026401 (2020).
[72] A. T. M. Anishur Rahman, and P. F. Barker, Optica **7**, 906 (2020).
[73] J. Fortágh and C. Zimmermann, Rev. Mod. Phys. **79**, 235 (2007).
[74] C. Gosse and V. Croquette, Biophys. J. **82**, 3314 (2002).
[75] E. Ostrofet, F. Stal Papini, and D. Dulin, Sci. Rep. **8**, 15920 (2018).
[76] K. Dholakia and P. Zemánek, Rev. Mod. Phys. **82**, 1767 (2010).
[77] Y. Arita, E. M. Wright, and K. Dholakia, Optica **5**, 910 (2018).
[78] H. S. Shi, H. X. Zheng, H. J. Chen, W. L. Lu, S. Y. Liu, and Z. F. Lin, Phys. Rev. A **101**, 043808 (2020).
[79] M. T. Wei, J. Ng, C. T. Chan, and H. D. Ou-Yang, Sci. Rep. **6**, 38883 (2016).
[80] S. Y. Liu, Z. Q. Yin, and T. C. Li, Adv. Quantum Technol. **3**, 1900099 (2020).
[81] J. Bang, R. Pan, T. M. Hoang, J. Ahn, C. Jarzynski, H. T. Quan and T. C. Li, New J. Phys. **20**, 103032 (2018).
[82] B. B. Hu, B. W. Li, and H. Zhao, Phys. Rev. E **57**, 2992 (1998).
[83] B. Q. Ai, D. H. He, and B. B. Hu, Phys. Rev. E **81**, 031124 (2010).
[84] H. Matsuda and K. Ishii, Suppl. Prog. Theor. Phys. **45**, 56 (1970).
[85] K. Ishii, Suppl. Prog. Theor. Phys. **53**, 77 (1973).
[86] J. B. Keller, G. C. Papanicolaou, and J. Weilenmann, Commun. Pure Appl. Math. **31**, 583 (1978).